

## A NUMERICAL MODEL ON THE INTERACTION BETWEEN NEARSHORE NONLINEAR WAVES AND STRONG CURRENTS

YE TIAN\* and SHINJI SATO†

*Department of Civil Engineering, The University of Tokyo,  
7-3-1 Hongo, Bunkyo-ku, Tokyo 113-8656, Japan*

\* *tianye@coastal.t.u-tokyo.ac.jp*

† *sato@coastal.t.u-tokyo.ac.jp*

Received 4 October 2007

Revised 9 June 2008

A new model for nearshore nonlinear water wave is established through the Galerkin Chebyshev spectral approach on the vertical direction. The model is based on the spatial-temporal separation conception. The Galerkin Chebyshev spectral approach is applied to solve the Laplace equation, while the Zakharov's expression of the free surface boundary condition is considered as the evolution equation of the free surface and integrated temporally. The accuracy and efficiency of the model are confirmed by the results of simulation of water waves over even bottom, nonlinear wave shoaling and harmonic generation over a submerged bar. Finally, the model is used to study the wave blocking phenomenon due to strong opposing currents. Both the location of the blocking point and the wave structure near the point are well presented.

*Keywords:* Chebyshev spectral approach; wave blocking; strong currents.

### 1. Introduction

The interaction between nearshore waves and currents is a very important and fundamental topic. As the natural consequence of the wave encountering strong opposing current, a striking nonlinear phenomenon called wave blocking often appears in the region of river mouth. The numerical study of the wave blocking phenomenon is necessary for a better understanding of the physical processes of nearshore hydrodynamics and morphological changes near the river mouth.

---

\*Corresponding author.

However, the numerical simulation of the wave blocking phenomenon demands efficacious numerical model which is capable of dealing with the inherent high non-linearity and large wave number of this problem. The classical Boussinesq equations (e.g. [Peregrine, 1967; Nwogu, 1993]) do not have a correct form of Doppler shift in connection with wave-current interaction. Chen *et al.* [1996] extended the Nwogu [1993]’s Boussinesq equations incorporating correct Doppler shift to simulate the wave transformation with a strong opposing current. However, their dispersion relation was not able to handle the large wave number generated by the ambient current. Strong bottom friction was also applied in order to stabilize the simulation, which eliminated the wave structures near the blocking point. Madsen *et al.* [1999] treated the case with the same computational conditions through their enhanced high order Boussinesq type equations and showed a great advancement.

Stimulated by the rapid advancement in the capacities of computer, inspired by Madsen’s enhanced Boussinesq type equations, the nonlinear mild slope equations by Isobe [1994] and the newly developed High Order Spectral method for the simulation of water waves from Mei *et al.* [2005], a new model is conceived and implemented for the 1DH cases in this study. The new model borrows the philosophy of eliminating the vertical coordinate with approximation of the flow field by the polynomials and the temporal-spatial decoupling-coupling scheme from the High Order Spectral method. Chebyshev polynomials are adopted to solve the spatial equation. The nonlinearity is dealt with high order.

It is expected that (1) the new model will greatly enhance the dispersion relation and nonlinear properties along with moderate increment of the need for computational resources, compared with conventional models, and (2) the 1DH model can be extended to 2DH without more theoretical treatment.

## 2. Physical description of the problem and governing equations

The physical domain of the nearshore flow field is described in Fig. 1. The continuous water body is enclosed by a free surface, a fixed bottom and two lateral boundaries.

Under the irrotational and inviscid assumption, potential flow theory is convenient for theoretical and numerical treatment. Define a Cartesian coordinate system  $\mathbf{r} \equiv (x, y, z)$ , and let  $(x, y) = \mathbf{x}$  be the horizontal coordinates,  $z$  the vertical coordinate, positive upward, and  $z = 0$  the mean free surface. The flow is described by a velocity potential  $\Phi(\mathbf{r}, t)$ , which satisfies the Laplace equation,

$$\nabla^2 \Phi(\mathbf{r}, t) = 0 \quad (1)$$

where  $\Phi(\mathbf{r}, t)$  is defined as  $\nabla \Phi(\mathbf{r}, t) = \mathbf{u}$ . On the free surface, the dynamic boundary condition can be written as (2),

$$\frac{\partial \Phi}{\partial t} + \frac{1}{2} |\nabla \Phi|^2 + gz = -\frac{P}{\rho} \quad (2)$$

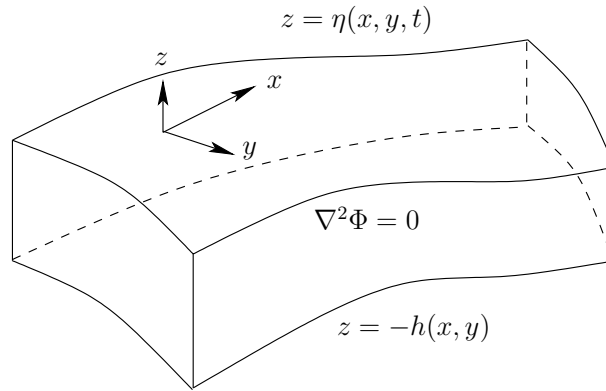


Fig. 1. Physical domain of the nearshore flow field.

where  $g$  is the acceleration of gravity,  $P$  is the pressure at the free surface, and  $\rho$  is the water density. Assume the free surface can be represented by  $z = \eta(\mathbf{x}, t)$  where  $\eta$  is a continuous and single-valued function of  $\mathbf{x}$ , that means that the wave is not overturned. The kinematic boundary condition is obtained as (3),

$$\eta_t + \nabla_x \eta \cdot \nabla_x \Phi - \Phi_z = 0, \quad z = \eta(\mathbf{x}, t) \quad (3)$$

where  $\nabla_x \equiv (\partial/\partial x, \partial/\partial y)$  denotes the horizontal gradient.

In the context of High-Order Spectral(HOS) Method and the newly developed high-order Boussinesq type Equations, the Zakharov [1968]'s expression of free surface boundary condition is favored. This re-arrangement of the original Eulerian form of free surface boundary conditions (2) and (3) is first derived by Zakharov [1968] when studying weakly-nonlinear slowly-modulated waves through the nonlinear Schrödinger equation [Zakharov, 1968].

As in Zakharov [1968], we define the potential on the free surface

$$\Phi^s(\mathbf{x}, t) \equiv \Phi(\mathbf{x}, \eta(\mathbf{x}, t), t) \quad (4)$$

Applying chain rules on (4):

$$\Phi_t(\mathbf{x}, \eta, t) = \Phi_t^s(\mathbf{x}, t) - \Phi_z(\mathbf{x}, \eta, t)\eta_t \quad (5)$$

$$\nabla_x \Phi(\mathbf{x}, \eta, t) = \nabla_x \Phi^s(\mathbf{x}, t) - \Phi_z(\mathbf{x}, \eta, t)\nabla_x \eta \quad (6)$$

The dynamic and kinematic free surface boundary conditions (2) and (3) can be rewritten as:

$$\begin{cases} \eta_t + \nabla_x \eta \cdot \nabla_x \Phi^s - (1 + \nabla_x \eta \cdot \nabla_x \eta)\Phi_z(\mathbf{x}, \eta, t) = 0 \\ \Phi_t^s + g\eta + \frac{1}{2}\nabla_x \Phi^s \cdot \nabla_x \Phi^s - \frac{1}{2}(1 + \nabla_x \eta \cdot \nabla_x \eta)\Phi_z^2(\mathbf{x}, \eta, t) = -\frac{P}{\rho} \end{cases} \quad (7)$$

An apparent advantage of using (7) instead of its original Eulerian form as free surface boundary conditions is that given the initial values of  $\eta$  and  $\Phi^s$ , (7) can be

directly integrated in time for the new values of  $\eta$  and  $\Phi^s$  as long as the surface vertical velocity  $\Phi_z(\mathbf{x}, \eta, t)$  is known. While the surface vertical velocity  $\Phi_z(\mathbf{x}, \eta, t)$  can be obtained by solving the Laplace equation (1) with the given  $\Phi^s$  as the Dirichlet boundary condition. At the bottom, the normal velocity of the flow is zero,

$$\frac{\partial \Phi}{\partial n} = 0 \quad (8)$$

where  $n$  is the normal direction of the boundary. If we define  $z = -h(\mathbf{x})$  to describe the topographic variation, (8) can be written as:

$$\Phi_z + \nabla_x h \cdot \nabla_x \Phi = 0, \quad z = -h(\mathbf{x}) \quad (9)$$

### 3. Galerkin Chebyshev Spectral Approach for the Laplace Equation

#### 3.1. Choice of base functions

The basic idea for solving differential equations through the spectral approach is to assume that the unknown function can be approximated by a linear combination of several “base functions”. With strategies to minimize the residual function, all the coefficients for the “base functions” are settled. It is important to choose a proper set of base functions.

An appropriate set of base function should be efficient, meaning that the results converge rapidly as the increase of the number of base functions. Here the hyperbolic functions cannot be considered to be a good candidate. Indeed the hyperbolic functions are the exact solutions of the Laplace equation, however, the appearance of the local wave number  $k$  weakens the efficiency of approximation. The local wave number is a function of space and period, and cannot be pre-determined. Therefore two schemes are adopted in literature. The first is using the dispersion relation of small amplitude wave theory directly, as in mild slope equation and Nadaoka [1994]’s attempt to extend it to the nonlinear cases; the second is the wide band simulation in HOS, which commonly utilizes 1,000 hyperbolic functions with wave number  $k$  from  $2\pi/L$  to  $1,000 \times 2\pi/L$ , where  $L$  is the length of the computational domain. The former is not able to represent the phenomena related to nonlinear shoaling and dispersion, and the latter obviously costs too many computational resources.

Well computational behavior is another requirement for obtaining creditable results. This requirement cannot be satisfied by the power functions. As increasing the number of base functions (the highest order of the power function), the condition number of the computational matrices will increase rapidly. In function approximation, the best square polynomial approximation of a given function with power functions to be the base functions generates the notorious Hilbert matrices, which are canonical examples of ill-conditioned matrices. Large computational error may be incurred by numerical round-off.

The shape of convergence domain is disadvantageous for the utilization of power functions as well. For power series, the domain shape is a disk, which means that

a singularity at the imaginary axis will make the model blow up. In fact, it really happens when deriving formula of cnoidal waves with power series expansion.

In recent development of the spectral methods for partial differential equations, Chebyshev orthogonal polynomial functions are frequently adopted. This set of functions is easy to compute, orthogonal, converges rapidly, and has a large convergence domain.

The Chebyshev polynomials of the first kind<sup>a</sup> are a set of orthogonal polynomials denoted as  $T_n(x)$ . The simplest definition of Chebyshev polynomials is the following recurrence relation:

$$\begin{aligned} T_0(x) &= 1 \\ T_1(x) &= x, \quad x \in [-1, 1] \\ T_{n+1}(x) &= 2xT_n(x) - T_{n-1}(x) \end{aligned} \quad (10)$$

The trigonometric definition (11) is convenient for the calculation with inner product.

$$T_n(\cos(\theta)) = \cos(n\theta) \quad (11)$$

The inner product along with Chebyshev polynomials is defined as:

$$(f, g) \equiv \int_{-1}^1 fg \frac{dx}{\sqrt{1-x^2}} \quad (12)$$

Therefore for a given function  $f(x) = a_i T_i(x)$ , the coefficient  $a_i$  can be expressed as:

$$a_i = \frac{2}{\pi c_i} (f, T_i) \quad (13)$$

where

$$c_i = \begin{cases} 2, & i = 0 \\ 1, & i \leq 1 \end{cases} \quad (14)$$

For the convenience of description, we define

$$\langle T_i, f \rangle \equiv \langle f, T_i \rangle \equiv \frac{2}{\pi c_i} (f, T_i) \quad (15)$$

### 3.2. Regulation of the computational domain

In order to expand the velocity potential to the Chebyshev series with respect to the vertical coordinate, we map the vertical computational domain  $z \in [-h(\mathbf{x}), \eta(\mathbf{x})]$  into  $s \in [-1, 1]$ . Therefore the uneven computational domain is mapped to a rectangle.

---

<sup>a</sup>Chebyshev polynomials mentioned in this paper are all abbreviated forms for Chebyshev polynomials of the first kind.

Denoting

$$h^+(\mathbf{x}) = h(\mathbf{x}) + \eta(\mathbf{x}) \tag{16}$$

$$h^-(\mathbf{x}) = h(\mathbf{x}) - \eta(\mathbf{x}) \tag{17}$$

$$s(\mathbf{x}) = \frac{2z + h^-(\mathbf{x})}{h^+(\mathbf{x})} \tag{18}$$

The velocity potential  $\Phi$  can be written as

$$\Phi(\mathbf{x}, z) = \Phi\left(\mathbf{x}, \frac{sh^+(\mathbf{x}) - h^-(\mathbf{x})}{2}\right) = \varphi(\mathbf{x}, s) \tag{19}$$

Using chain rules on the Laplace equation (1), we obtain

$$h^+(\mathbf{x})^2 \nabla^2 \varphi(\mathbf{x}, s) = m_{ijk} s^i \frac{\partial^{j+k}}{\partial \mathbf{x}^j \partial s^k} \varphi(\mathbf{x}, s) = 0, \quad i = 0, 1, 2; j + k \leq 2 \tag{20}$$

where

$$m_{020} = (h^+)^2 \tag{21}$$

$$m_{111} = -2h^+ \nabla_x h^+ . \tag{22}$$

$$m_{011} = 2h^+ \nabla_x h^- . \tag{23}$$

$$m_{101} = 2(\nabla_x h^+)^2 - h^+ \nabla_x^2 h^+ \tag{24}$$

$$m_{001} = -2\nabla_x h^- \cdot \nabla_x h^+ + h^+ \nabla_x^2 h^- \tag{25}$$

$$m_{202} = (\nabla_x h^+)^2 \tag{26}$$

$$m_{102} = -2\nabla_x h^- \cdot \nabla_x h^+ \tag{27}$$

$$m_{002} = (\nabla_x h^-)^2 + 4 \tag{28}$$

The  $m_{ijk}$  not mentioned from (21) to (28) is equal to 0.

### 3.3. Chebyshev series expansion for regulated Laplace equation

The target unknown function  $\varphi(\mathbf{x}, s)$  can be approximated as  $\varphi_N(\mathbf{x}, s)$

$$\varphi_N(\mathbf{x}, s) = \sum_{n=0}^N a_n(\mathbf{x}) T_n(s) \tag{29}$$

Denoting the differential operator in (20) as

$$\mathcal{L}_{ijk} = s^i \frac{\partial^{j+k}}{\partial \mathbf{x}^j \partial s^k} \tag{30}$$

we obtain

$$\mathcal{L}_{ijk}\varphi_N(\mathbf{x}, s) = \sum_{n=0}^N \frac{\partial^j}{\partial \mathbf{x}^j} a_n(\mathbf{x}) s^i \frac{\partial^k}{\partial s^k} T_n(s) \tag{31}$$

Therefore the coefficients of the residual function of (20) can be written as:

$$r_p = \langle T_p(s), m_{ijk}\mathcal{L}_{ijk}\varphi_N(\mathbf{x}, s) \rangle = \sum_{n=0}^N m_{ijk} \frac{\partial^j}{\partial \mathbf{x}^j} a_n(\mathbf{x}) \left\langle T_p(s), s^i \frac{\partial^k}{\partial s^k} T_n(s) \right\rangle \tag{32}$$

$p = 0, 1, \dots, N$

where the last pair of parentheses is a 4-dimensional tensor denoted as

$$\mathcal{B}_{pikn} = \left\langle T_p(s), s^i \frac{\partial^k}{\partial s^k} T_n(s) \right\rangle \tag{33}$$

The values of  $\mathcal{B}_{pikn}$  can be determined analytically.

### 3.4. Boundary conditions

#### 3.4.1. Free surface boundary conditions

For the free surface,  $\Phi^s$  of the present time is already given. Thus, the Dirichlet type boundary condition can be written as:

$$\sum_{n=0}^N a_n(\mathbf{x}) T_n(s)|_{s=1} = \sum_{n=0}^N a_n(\mathbf{x}) = \Phi^s(\mathbf{x}) \tag{34}$$

#### 3.4.2. Bottom boundary condition

Applying chain rules on (29), we obtain

$$\nabla_x \varphi_N = \nabla_x a_n T_n + a_n \frac{dT_n}{ds} \frac{\nabla_x h^- - s \nabla_x h^+}{h^+} \tag{35}$$

Substituting (35) into (9) and evaluating at  $s = -1$ , we obtain

$$2a_n n^2 (-1)^{n-1} \frac{(\nabla_x h)^2 + 1}{h^+} + (-1)^n \nabla_x a_n \cdot \nabla h = 0 \tag{36}$$

#### 3.4.3. Incident lateral boundary

The incident waves are formulated through Stream Function Wave theory [Dean, 1965]. Therefore, both the velocity  $u_I$  and velocity potential  $\Phi_I$  of the incident wave are represented in the following form:

$$\sum_{i=1}^M X_i(\mathbf{x}, t) \cosh ik(z + h) = \sum_{i=1}^M X_i(\mathbf{x}, t) \cosh \frac{ik(s + 1)h^+}{2} \tag{37}$$

Chebyshev series expansion of (37) arouses the following integration:

$$\int_{-1}^1 \frac{\cosh[ik(s+1)h^+/2]}{\sqrt{1-s^2}} T_n(s) ds = \begin{cases} \pi I_n(ikh^+/2) \cosh[ikh^+/2], & n = 0, 2, 4, \dots \\ \pi I_n(ikh^+/2) \sinh[ikh^+/2], & n = 1, 3, 5, \dots \end{cases} \quad (38)$$

where  $I_n$  is the  $n$ th order modified Bessel function of the first kind.

### 3.4.4. Far-field conditions

For an impermeable, reflective vertical wall, the far-field condition is simple as:

$$\nabla_x \Phi = 0 \quad (39)$$

Applying Galerkin approach to (35), we obtain

$$\nabla_x a_p + \sum_{n=0}^N a_n \left( \frac{\nabla_x h^-}{h^+} \mathcal{B}_{p01n} - \frac{\nabla_x h^+}{h^+} \mathcal{B}_{p11n} \right) = 0, \quad p = 0, 1, \dots, N \quad (40)$$

The open boundary condition for the spectral approach described in this study has been treated with great care. Although there are many scheme (e.g. [Larsen and Dancy, 1983]) to make an open boundary, most of them are designed for equations using the original variables  $\mathbf{u}, \eta$ . For the approach using the velocity potential, those scheme cannot make satisfactory results. Ohyama [1991] proposed a numerical wave absorber for a Mixed Euler-Lagrangian (MEL) method which uses the velocity potential as a variable. Figure 2 shows a schematic diagram of the numerical wave-absorption filter. An artificial “sponge layer” with gradually increasing damping coefficient is attached to the computational domain, where  $\mu$  is the damping coefficient in the “sponge layer” and  $x_{sp0}, x_{sp1}$  are the location of the beginning and end of the “sponge layer”. Due to the inefficiency of the “sponge layer” to absorb long wave, behind the “sponge layer”, a radiation boundary condition is set in order to allow long waves propagating out of the “sponge layer”. Following Ohyama’s idea, we obtain the free surface boundary condition over the sponge layer:

$$\begin{cases} \eta_t + \nabla_x \eta \cdot \nabla_x \Phi^s - (1 + \nabla_x \eta \cdot \nabla_x \eta) \Phi_z(\mathbf{x}, \eta, t) = 0 \\ \Phi_t^s + g\eta + \frac{1}{2} \nabla_x \Phi^s \cdot \nabla_x \Phi^s - \frac{1}{2} (1 + \nabla_x \eta \cdot \nabla_x \eta) \Phi_z^2(\mathbf{x}, \eta, t) \\ \quad + \mu \Phi^s - \int_{x_{sp0}}^{x_{sp1}} \Phi^s \nabla_x \mu \cdot d\mathbf{x} = -\frac{P}{\rho} \end{cases} \quad (41)$$

Behind the “sponge layer”, the wave is assumed as long wave. The radiative boundary condition is written as

$$\nabla_x a_0 = \frac{\eta \sqrt{gh}}{h}, \quad x = x_{sp1} \quad (42)$$

where  $\sqrt{gh}$  is the wave celerity of long wave.

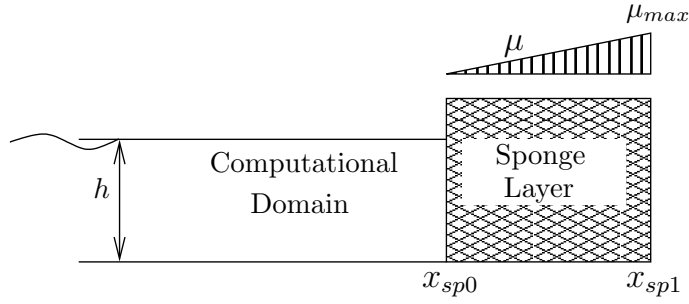


Fig. 2. Schematic diagram of the numerical wave-absorption filter.

### 3.5. Summary of governing equations

For the convenience of description, the equations for the 1DH case is summarized here. The whole time-dependent problem after the Galerkin spectral approach is written as follows:

#### Evolution equations for the free water surface

$$\left\{ \begin{array}{l} \eta_t + \nabla_x \eta \cdot \nabla_x \Phi^s - (1 + \nabla_x \eta \cdot \nabla_x \eta) \Phi_z(\mathbf{x}, \eta, t) = 0 \\ \Phi_t^s + g\eta + \frac{1}{2} \nabla_x \Phi^s \cdot \nabla_x \Phi^s - \frac{1}{2} (1 + \nabla_x \eta \cdot \nabla_x \eta) \Phi_z^2(\mathbf{x}, \eta, t) = -\frac{P}{\rho}, x < x_{sp0} \\ \Phi_t^s + g\eta + \frac{1}{2} \nabla_x \Phi^s \cdot \nabla_x \Phi^s - \frac{1}{2} (1 + \nabla_x \eta \cdot \nabla_x \eta) \Phi_z^2(\mathbf{x}, \eta, t) \\ + \mu \Phi^s - \int_{x_{sp0}}^{x_{sp1}} \Phi^s \nabla_x \mu \cdot d\mathbf{x} = -\frac{P}{\rho}, x > x_{sp0} \end{array} \right. \quad (43)$$

#### Continuity equation in the computational domain

$$\sum_{n=0}^N m_{ijk} \frac{\partial^j}{\partial \mathbf{x}^j} a_n(\mathbf{x}) \mathcal{B}_{pikn} = 0, \quad p = 0, 1, \dots, N-2 \quad (44)$$

#### Dirichlet boundary condition for free surface

$$\sum_{n=0}^N a_n(\mathbf{x}) = \Phi^s(\mathbf{x}) \quad (45)$$

#### Impermeable boundary condition for the bottom

$$2a_n n^2 (-1)^{n-1} \frac{(\nabla_x h)^2 + 1}{h^+} + (-1)^n \nabla_x a_n \cdot \nabla h = 0 \quad (46)$$

#### Lateral boundary condition for incident waves

Dirichlet

$$a_n = \langle T_n, \varphi_i \rangle, \quad n = 0, 1, \dots, N \quad (47)$$

Neumann boundary condition

$$\nabla_x a_p + \sum_{n=0}^N a_n \left( \frac{\nabla_x h^-}{h^+} \mathcal{B}_{p01n} - \frac{\nabla_x h^+}{h^+} \mathcal{B}_{p11n} \right) = \langle T_p, \mathbf{u}_i \rangle, \quad p = 0, 1, \dots, N \quad (48)$$

**Far field condition**

Impermeable vertical wall

$$\nabla_x a_p + \sum_{n=0}^N a_n \left( \frac{\nabla_x h^-}{h^+} \mathcal{B}_{p01n} - \frac{\nabla_x h^+}{h^+} \mathcal{B}_{p11n} \right) = 0, \quad x_0 = +\infty \quad p = 0, 1, \dots, N \quad (49)$$

Open boundary

$$\nabla_x a_0 = \frac{\eta \sqrt{gh}}{h} \quad (50)$$

Up to now, the main part of the theoretical derivation is completed. The following section will discuss the numerical implementation of this model.

**4. Numerical Implementation**

Through Galerkin approach, the vertical coordinate in the governing equations has been eliminated. All the differential operators are applied to the horizontal coordinates. It is then possible to obtain a solvable system with spectral or pseudo-spectral methods on the two horizontal coordinates. However, the benefits of applying spectral methods to the horizontal coordinates is not so significant as to the vertical coordinate. The 10th order Chebyshev polynomials on the vertical coordinate will satisfy most of the requirements, while the 1,000th order may be necessary for the horizontal coordinates. Surely a full spectral solver will greatly enhance the accuracy of the results and efficiently save the numbers of unknowns, yet the full spectral approach always induces full matrices, which cost much memory to store and computational time to factorize. Therefore, it is difficult to evaluate the loss and gain.

Although with shortage of accuracy and efficiency, the finite difference scheme has several merits. It is easy to program, flexible to carry out local procedures (e.g. to multiply damping coefficient on a certain term) and generates band diagonal matrices. The 1-dimensional solver is also convenient to extend to 2-dimensional problem, which is a really tedious work for the full spectral solver.

After weighing those factors mentioned above, in an attempt of this study, we adopt a semi-spectral solver, which utilizes the finite difference scheme along the horizontal 1 dimension cases. A schematic diagram for solving (43) to (50) is shown in Fig. 3.

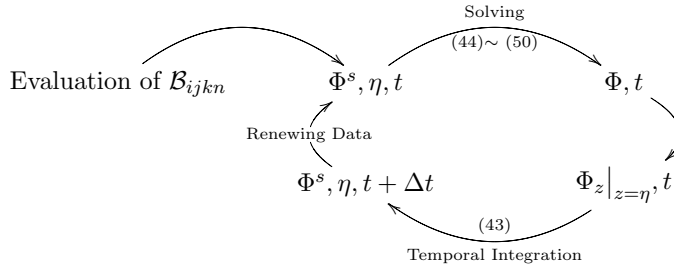


Fig. 3. Schematic diagram for solving (43) to (50).

#### 4.1. Evaluation of $\mathcal{B}_{ijkn}$

As shown in Fig. 3, the tensor  $\mathcal{B}_{ijkn}$  is evaluated before the main loop of temporal integration. All the evaluations are based on three fundamental values:

$$\mathcal{B}_{i00n} = \langle T_i, T_n \rangle = \begin{cases} 0, & i \neq n \\ 1, & i = n \end{cases} \quad (51)$$

$$\mathcal{B}_{i01n} = \langle T_i, dT_n/ds \rangle = \frac{2}{c_i} \begin{cases} n, & i \in \{n-1, n-3, n-5, \dots\} \\ 0, & \text{otherwise} \end{cases} \quad (52)$$

$$\mathcal{B}_{i02n} = \langle T_i, d^2T_n/ds^2 \rangle = \frac{1}{c_i} \begin{cases} n(n^2 - i^2), & i \in \{n-2, n-4, n-6, \dots\} \\ 0, & \text{otherwise} \end{cases} \quad (53)$$

Thus,  $dT_n/ds$  and  $d^2T_n/ds^2$  can be expressed as

$$\frac{dT_n}{ds} = \sum_{i=0}^{n-1} \mathcal{B}_{i01n} T_i \quad (54)$$

$$\frac{d^2T_n}{ds^2} = \sum_{i=0}^{n-2} \mathcal{B}_{i02n} T_i \quad (55)$$

From the recursive definition of Chebyshev Polynomials (10), we obtain

$$sT_k(s) = \begin{cases} \frac{T_{k-1} + T_{k+1}}{2}, & k \geq 1 \\ T_1, & k = 0 \end{cases} \quad (56)$$

and

$$s^2 T_k(s) = \begin{cases} \frac{T_{k-2} + 2T_k + T_{k+2}}{4}, & k \geq 2 \\ \frac{3T_1 + T_3}{4}, & k = 1 \\ \frac{T_0 + T_2}{2}, & k = 0 \end{cases} \tag{57}$$

Substituting (56) and (57) into (54) and (55), and applying (51)–(53) we can evaluate all the other  $\mathcal{B}_{ijkn}$ 's.

Take  $\mathcal{B}_{i11n}$  as an example:

$$s \frac{dT_n}{ds} = \sum_{r=0}^{n-1} \mathcal{B}_{r01n} \begin{cases} \frac{T_{r-1} + T_{r+1}}{2}, & r \geq 1 \\ T_1, & r = 0 \end{cases} \tag{58}$$

Therefore

$$\begin{aligned} \mathcal{B}_{i11n} &= \left\langle T_i, s \frac{dT_n}{ds} \right\rangle \\ &= \left\langle T_i, \sum_{r=0}^{n-1} \mathcal{B}_{r01n} \begin{cases} \frac{T_{r-1} + T_{r+1}}{2}, & r \geq 1 \\ T_1, & r = 0 \end{cases} \right\rangle \\ &= \sum_{r=0}^{n-1} \mathcal{B}_{r01n} \begin{cases} \frac{\langle T_i, T_{r-1} \rangle + \langle T_i, T_{r+1} \rangle}{2}, & r \geq 1 \\ \langle T_i, T_1 \rangle, & r = 0 \end{cases} \\ &= \sum_{r=0}^{n-1} \mathcal{B}_{r01n} \begin{cases} \frac{\mathcal{B}_{i00(r-1)} + \mathcal{B}_{i00(r+1)}}{2}, & r \geq 1 \\ \mathcal{B}_{i001}, & r = 0 \end{cases} \end{aligned} \tag{59}$$

By the similar virtue, all the  $\mathcal{B}_{ijkn}$  are able to be evaluated.

#### 4.2. Spatial discretization

By knowing the value of  $\mathcal{B}_{ijkn}$ , spatial discretization can be carried out. The unknowns are the coefficients of the Chebyshev polynomials,  $a_n(x)$ . A non-staggered mesh is adopted.

Equation (44) can be written as

$$\frac{\partial^2 a_n}{\partial \mathbf{x}^2} + \sum_{m=0}^N \mathcal{C}(\mathbf{x})_{nm} \frac{\partial a_m}{\partial \mathbf{x}} + \sum_{m=0}^N \mathcal{D}(\mathbf{x})_{nm} a_m = 0, \quad n = 1, 2, \dots, N - 2 \tag{60}$$

where  $\mathcal{C}(\mathbf{x})$  and  $\mathcal{D}(\mathbf{x})$  are coefficient matrices.

For the first term in (44), the 2nd order central difference scheme is applied:

$$\left(\frac{\partial^2 a_n}{\partial x^2}\right)^i = \frac{a_n^{i+1} - 2a_n^i + a_n^{i-1}}{\Delta x^2}, \quad O(\Delta x^2) \tag{61}$$

For the second term in (44), the difference scheme changes with the  $m$  subscript. If  $m = n$ , we adopt the second order upwind difference scheme:

$$\left(\frac{\partial a_m}{\partial x}\right)^i = \begin{cases} \frac{1}{2\Delta x}(3a_m^i - 4a_m^{i-1} + a_m^{i-2}), & O(\Delta x^2), \quad C_{nm} < 0 \\ \frac{1}{2\Delta x}(-3a_m^i + 4a_m^{i+1} - a_m^{i+2}), & O(\Delta x^2), \quad C_{nm} > 0 \end{cases} \tag{62}$$

If  $m \neq n$ , the second order central difference scheme is applied:

$$\left(\frac{\partial a_m}{\partial x}\right)^i = \frac{1}{2\Delta x}(a_m^{i+1} - a_m^{i-1}), \quad O(\Delta x^2) \tag{63}$$

### 4.3. Incident boundary conditions

In the first few periods, a moderation coefficient  $\alpha(t)$  is multiplied to the incident conditions.

$$\alpha = 1 - \exp\left(-\beta \frac{t}{T}\right) \tag{64}$$

where  $\beta$  is usually set to 1. Thus a tentative incident boundary condition is adopted:

$$\Phi_I^{st} = \alpha(t)\Phi_I \tag{65}$$

$$u_I^{st} = \alpha(t)u_I \tag{66}$$

$$\eta_I^{st} = \alpha(t)\eta_I \tag{67}$$

#### 4.3.1. Dirichlet boundary condition

For the Dirichlet boundary condition, another factor has to be considered. From (7) and (1) we can find that those equations still hold after adding a constant  $C$  on  $\Phi$ . That means there may be a spatial constant difference between  $\Phi_I$  and  $\Phi_{cal}$  due to different datums (The datum for the velocity potential from stream function theory is a moving point  $x - ct = 0$ , while the datum for the velocity potential in the computational domain is a fixed point located at  $x = +\infty$ ). Fortunately the 0th order Chebyshev polynomials  $T_0$  is a constant value 1, meaning that the vertical derivative  $\Phi_z$  will not be influenced by the coefficient before  $T_0$ . Therefore we use the value  $(T_1, \Phi_i), (T_2, \Phi_i), \dots$ , only leaving the  $T_0$  for a derivative-type relation in order to eliminate the inconsistency due to the difference between datums.

$$\begin{aligned} -1.5a_0^0 - 2a_0^1 - 0.5a_0^2 &= \langle T_0, \mathbf{u}(x_0) \rangle \\ -1/6a_0^0 + a_0^1 - 0.5a_0^2 - 1/3a_0^3 &= \langle T_0, \mathbf{u}(x_1) \rangle \end{aligned} \tag{68}$$

$$\begin{aligned} a_n^0 &= \langle T_n, \Phi(x_0)_I \rangle, \quad n = 1, 2, \dots, N \\ a_n^1 &= \langle T_n, \Phi(x_1)_I \rangle, \quad n = 1, 2, \dots, N \end{aligned} \tag{69}$$

4.3.2. *Neumann boundary condition*

The Neumann boundary condition is simple as follows:

$$\begin{aligned} -1.5a_p^0 - 2a_p^1 - 0.5a_p^2 + \sum_{n=0}^N a_n^0 \left( \frac{\nabla_x h^-}{h^+} \mathcal{B}_{p01n} - \frac{\nabla_x h^+}{h^+} \mathcal{B}_{p11n} \right) &= \langle T_p, \mathbf{u}_I \rangle, \\ p &= 0, 1, \dots, N \end{aligned} \tag{70}$$

$$\begin{aligned} -1/6a_p^0 + a_p^1 - 0.5a_p^2 - 1/3a_p^3 \sum_{n=0}^N a_n^0 \left( \frac{\nabla_x h^-}{h^+} \mathcal{B}_{p01n} - \frac{\nabla_x h^+}{h^+} \mathcal{B}_{p11n} \right) &= \langle T_p, \mathbf{u}_I \rangle, \\ p &= 0, 1, \dots, N \end{aligned}$$

***Impermeable reflective boundary condition***

From (49), we simply obtain

$$\begin{aligned} 1.5a_p^{N-1} - 2a_p^{N-2} + 0.5a_p^{N-3} + \sum_{n=0}^N a_n^{N-1} \left( \frac{\nabla_x h^-}{h^+} \mathcal{B}_{p01n} - \frac{\nabla_x h^+}{h^+} \mathcal{B}_{p11n} \right) &= 0, \\ p &= 0, 1, \dots, N \end{aligned} \tag{71}$$

***Open boundary condition***

$$1.5a_0^{N-1} - 2a_0^{N-2} + 0.5a_0^{N-3} = \frac{\eta\sqrt{gh}}{h} \tag{72}$$

4.4. ***Analysis of the linear algebra system***

The linear algebra system generated from the above discretization approach is a blocked sparse matrix. The distribution of the non-zero element is shown in Fig. 4. We can find that the matrix consists of several  $(N + 1) \times (N + 1)$  block. Exactly speaking, it is a band diagonal matrix with band width  $2 \times (N + 1)$ . The LAPACK routines for solving band diagonal linear algebra system is adopted. Denoting the number of total points is  $N_p$ , the routine for *LU* factorization in LAPACK named DGBTRF, carries out approximately  $2N_p(2N + 1)(2N + 2) \sim 2N_p(2N + 1)(4N + 3)$  times of floating-point operations, depending on the interchanges. Routine for forward and backward substitution to solve the equation named DGBTRS precedes  $2N_p(6N + 3)$  times floating-point operations. Therefore, the temporal complexity for the spatial solving approach can be estimated as  $O(N_p N^2)$ . Compared with full



Fig. 4. Distribution of the non-zero element of the LAS for 1DH.

matrix which arouses a temporal complexity of  $O(N_p^3)$ , the present scheme saves the computational time significantly at least for 1DH cases.

It is necessary to point out that although a compact band matrix can be obtained for the 1DH case, the matrix elements must be scattered for the 2DH, which may reduce computational efficiency. The Alternative-Direction-Implicit(ADI) scheme is expected to be applied to the 2DH cases in order to enhance the computational efficiency.

**4.5. Temporal integration and calculation of vertical derivatives**

The temporal integration of (43) is carried out through the 4th order Runge-Kutta method without too much difficulty.

While a key value in (43) is  $\Phi_z$ , which is also easy to be calculated as follows.

$$\frac{ds}{dz} = \frac{2}{h^+} \tag{73}$$

Applying the chain rule, we obtain

$$\begin{aligned} \Phi_z &= \frac{2}{h^+} \sum_{n=0}^N a_n \frac{dT_n(s)}{ds} \\ &= \frac{2}{h^+} \sum_{n=1}^N a_n n^2 \end{aligned} \tag{74}$$

### 5. Model Verification

In order to verify the model, we use the model to simulate three phenomena: the propagation of finite amplitude waves over an even bottom with different relative water depth and wave number; nonlinear wave shoaling; harmonic generation for waves propagating over a submerged breakwater. The first two cases have theoretical solutions which can be used as the criteria and in the third case the result of simulation will be compared with laboratory data, and with the results from Boussinesq-type models. The 12th order Chebyshev polynomial is adopted in all the simulations.

#### 5.1. Waves on horizontal bottom

For the waves on a horizontal bottom, two cases of incident waves have been selected. The first case is the test of short wave and the second case is the test of nonlinear wave in the intermediate water depth. The characteristic parameters of the incident waves are listed in Table 1.

Table 1. Characteristic parameters of the incident waves.

	$T(s)$	$h(m)$	$H(m)$	$\Delta t(s)$
case 1	0.6	1.0	0.001	0.01
case 2	5.0	1.0	0.3	0.1

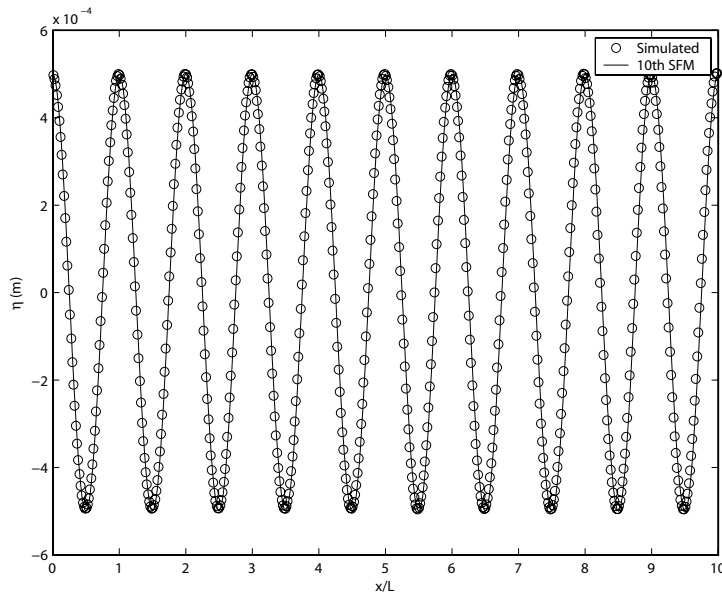


Fig. 5. Spatial distribution for calculated surface elevation,  $kh = 11$ .

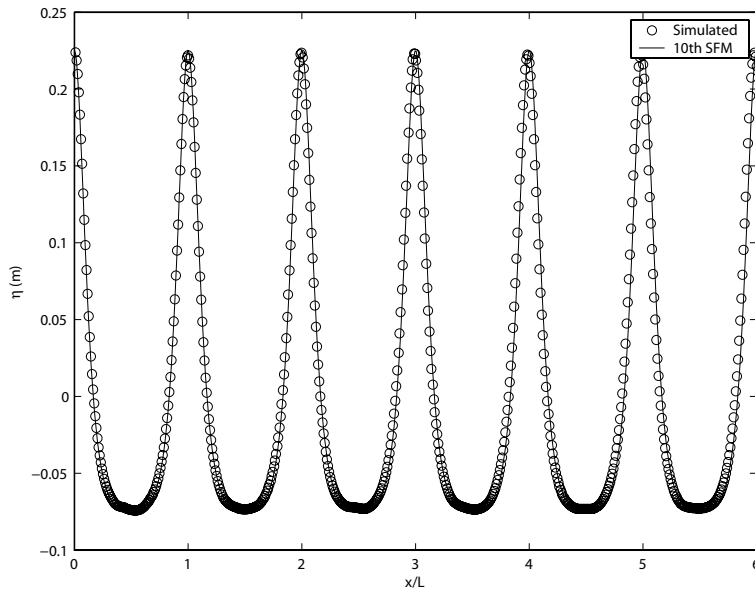


Fig. 6. Spatial distribution for calculated surface elevation,  $H/h = 0.3$ .

Table 2. Computational conditions for different cases of shoaling study.

Case	$H_0/L_0$	$h_1$ [m]	$h_2$ [m]	$K_{S1}$	$H_1/2$ [m]	Slope Length[m]	Slope
1	0.001	1.0	0.5	1.6	0.08	50	0.01
2	0.005	6.0	1.37	1.0071	0.2518	463	0.01

Figures 5 and 6 demonstrate the spatial distribution of the water surface elevation for cases 1 and 2, comparing with the analytical results from the 10th order Stream Function wave theory. In both figures, the difference between the numerical simulation and the theory cannot be easily recognized. Here it is pointed out that for the short wave in case 1, the results from most of the Boussinesq type equations will have significant phase shift referring to the theoretical solution.

### 5.2. Nonlinear wave shoaling

In order to examine the ability of this model to predict wave shoaling over slowly varying depth, two incident waves and their corresponding shoaling conditions are listed in Table 2, where  $h_1$  is the offshore depth,  $h_2$  the onshore depth,  $H_1$  the offshore wave height calculated from the deepwater wave height  $H_0$ , using the linear wave theory shoaling coefficient  $K_s$ . Figure 7 shows a sketch for the computational domain used in this study.

The shoaling coefficients are calculated, and compared with the results of Stiassnie and Peregrine [1980] and Shuto [1974] in Figs. 8 and 9. It is clear from these

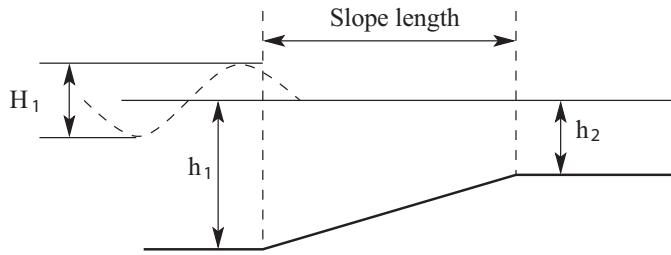


Fig. 7. Spatial distribution for calculated surface elevation, wave height, and bottom depth.

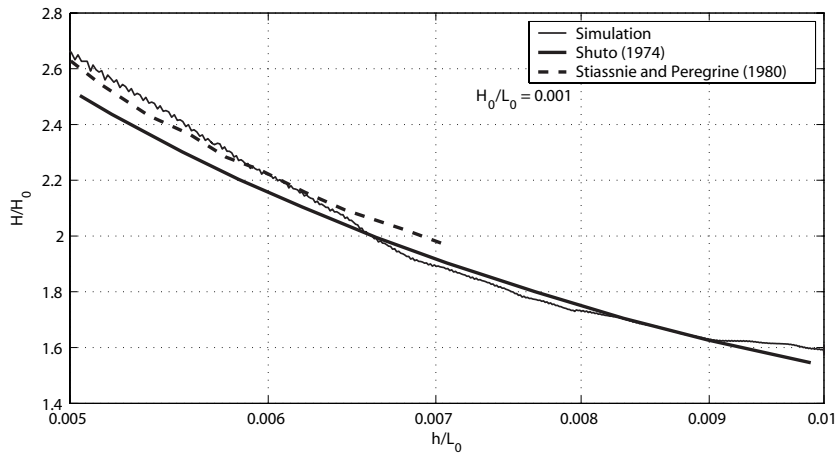


Fig. 8. Shoaling coefficient obtained by the present model, Stiassnie and Peregrine [1980] and Shuto [1974].

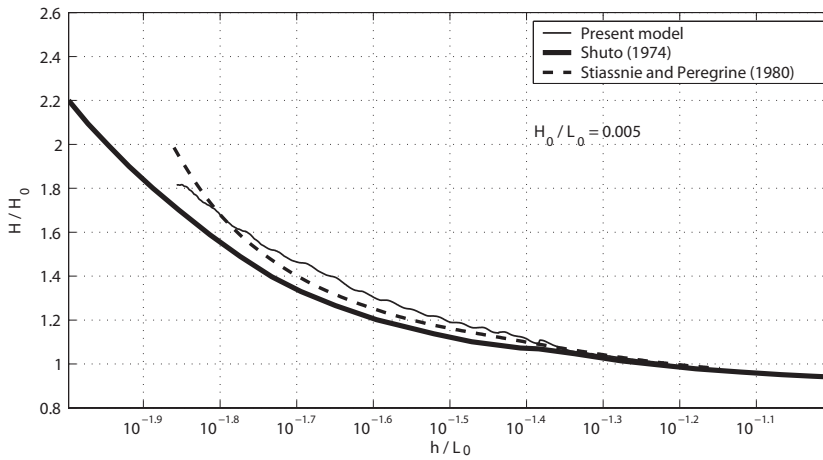


Fig. 9. Shoaling coefficient obtained by the present model, Stiassnie and Peregrine [1980] and Shuto [1974].

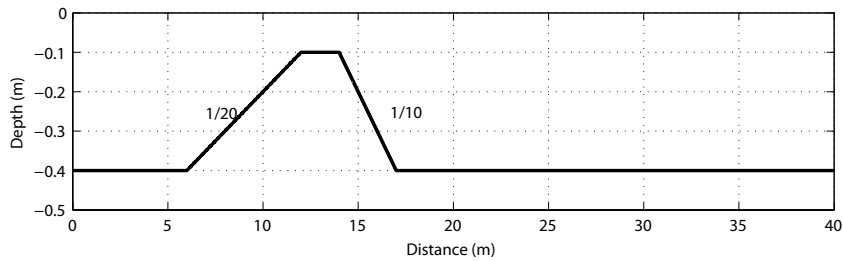


Fig. 10. Bathymetry of Luth's experiment.

figures that the model developed through Chebyshev Spectral approach has a good capability to simulate water wave shoaling over slowly varying topography.

### 5.3. Harmonic generation for waves propagating over a submerged breakwater

Wave transformation over submerged bars in shallow water is an intriguing problem, which involves the phenomena of wave-wave interaction and harmonic generation. Here we simulate the experiment by Luth [1994]. The experiments were equivalent to the set up of Beji and Battjes [1993] except for a factor 2 scaling. In the reduced scale the bathymetry is defined as shown in Fig. 10, a horizontal flume with a depth of 40 cm, a trapezoidal bar with an upward slope of  $1/20$ , a downward slope of  $1/10$ , and a depth of 10 cm on top of the bar. Active absorption was applied at both ends of the flume. Their test case *A* is used for the verification in the following. Case *A* is based on regular incident waves with a wave period of 2.02 s and a wave height of 2.0 cm.

Figures 11 to 13 show the the simulated time series of surface elevations at three locations, together with the simulation by Madsen [1999] for the same condition using Nwogu [1993] and Wei and Kirby [1995]'s equation. From Figs. 11 to 13, the agreement between the simulation and measurement is fair. The slight overshooting of the wave height for the first order harmonic wave is related to the lack of dissipation of the model, while either Wei [1995]'s or Nwogu [1993]'s model fails to simulate the harmonic generation at the location where  $x = 19$  m and  $x = 21$  m. The main reason for the success of the model in this study is believed to be due to its fully-nonlinear characteristics and high accuracy to describe shoaling and dispersion.

## 6. Numerical Study of Nonlinear Wave/Current Interaction

After the model verification via different computational conditions, the reliability and accuracy of the model have been confirmed. The direct application of the model is the numerical study of nonlinear wave-current interaction. This study focuses in particular on the numerical simulation for wave blocking phenomenon.

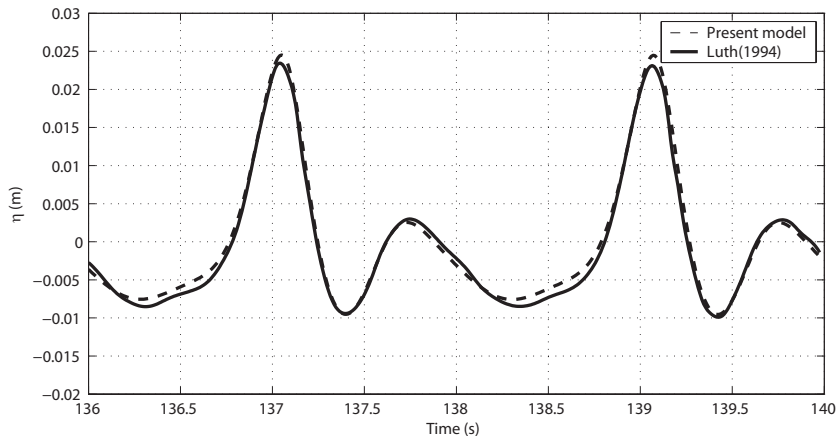


Fig. 11. Harmonic generation over a submerged bar,  $x = 14.5$  m.

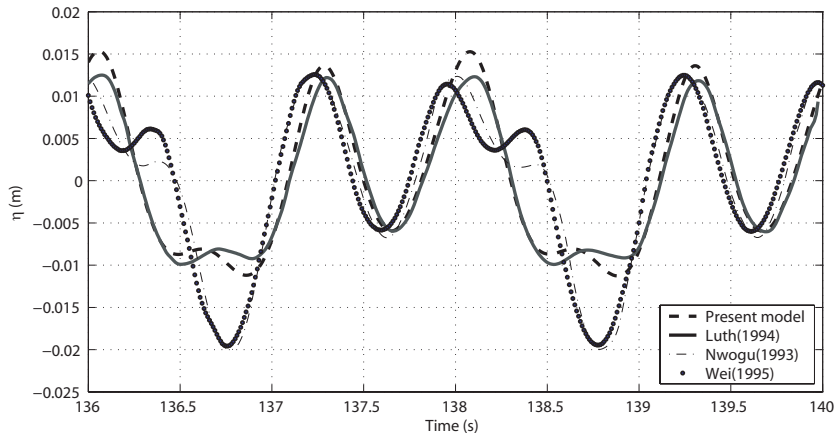


Fig. 12. Harmonic generation over a submerged bar,  $x = 19$  m.

### 6.1. *Simulation for wave blocking phenomenon*

Here it is necessary to elucidate the condition of the wave blocking phenomenon again: when propagating waves encounter an opposing current of increasing magnitude, wave blocking phenomenon occurs at a place where the current speed matches the group velocity of the wave. In the blocking region, the wave becomes shorter and steeper, and eventually breaks as it is reflected and travels back.

In the small amplitude wave theory, an explanation from the perspective of energy is that: when a wave train encounters a current in which the surface velocity varies, the excess momentum flux results in an interchange of energy between waves and current. When the convection velocity of energy is equal and opposite to the local group velocity of the waves, the energy can no longer be propagated against the stream and accumulated before the breaking point. The accumulation of the

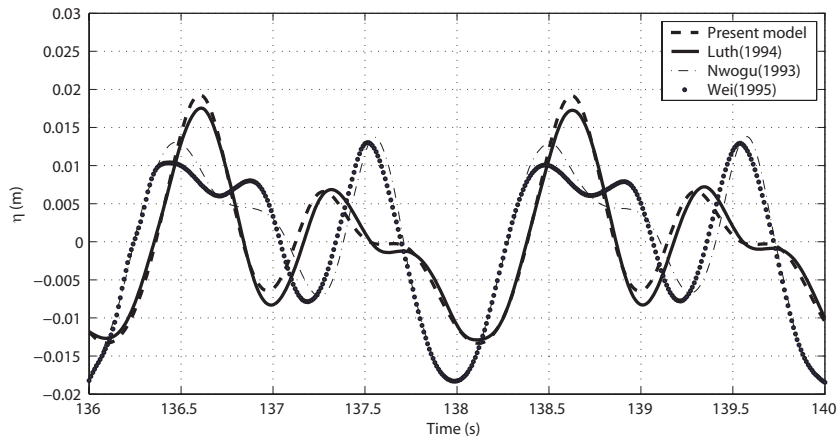


Fig. 13. Harmonic generation over a submerged bar,  $x = 21$  m.

energy leads to infinite wave amplitude which is unrealistic and appears in the form of wave breaking (e.g. [Longuet-Higgins and Stewart, 1961]; [Phillips, 1977]).

Analytical and semi-analytical studies of the nonlinear wave blocking phenomenon point out that the breaking of wave before the blocking point is in the form of reflection and backward travel of waves with high wave number (e.g. [Smith, 1975]; [Shyu and Phillips, 1990]; [Shyu and Tung, 1999]). However, theoretical treatment for wave blocking by Peregrine and Thomas [1979] does not include the effect of wave reflection and fails in the blocking region where the assumption of slowly varying waves breaks down.

Numerical approaches for the wave blocking phenomenon have been carried out by Chen [1996] through a set of modified Boussinesq equations. A current-wave separation skill was applied to Nwogu [1993]'s Boussinesq equation with length scale parameters. However, this approach requires a very strong bottom friction in order to stabilize simulation. The strong dissipation introduced by the bottom friction remove all the key structures near the blocking point.

## 6.2. Computational conditions

In this study, similar computational conditions as in Chen [1996] are adopted. The spatial variation of current is generated by spatial change of topography. This case considers a wave train propagating against a current in a channel with a submerged bar. A sketch of the bathymetry is shown in Fig. 14.

The channel is 60 m long, 0.8 m deep on both sides of the bar and 0.2 m deep on top of the bar. The bar is located from 8.0 m to 55.0 m. The slopes of the bar are 1/50 on the incoming side and 1/20 on the transmission side. The two corners of the bar near  $x = 40$  m are rounded for the convenience to obtain the initial boundary conditions.

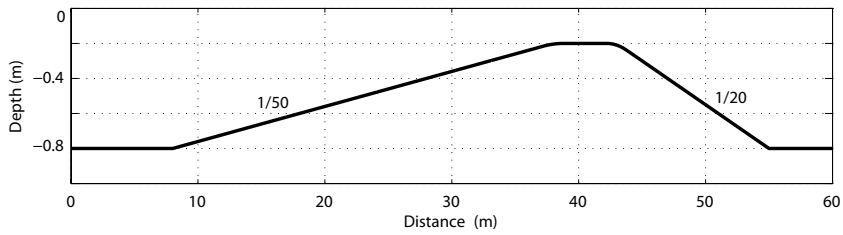


Fig. 14. Bathymetry of the channel.

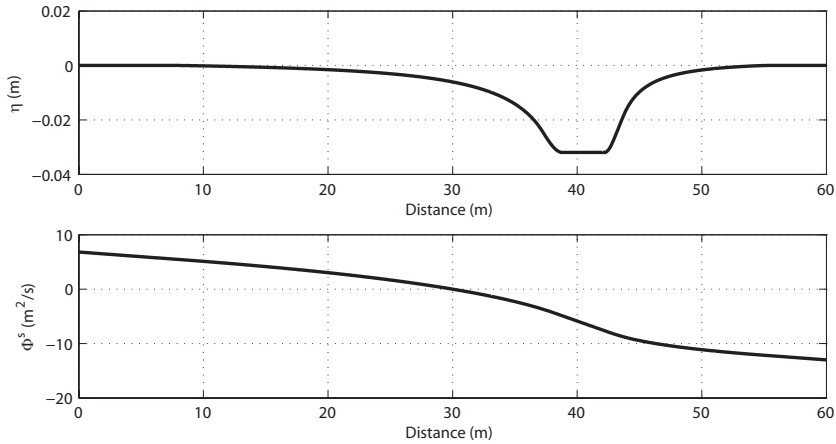


Fig. 15. Initial spatial distribution of water elevation, and velocity potential.

The depth uniform steady current has a discharge of  $-0.136 \text{ m}^2/\text{s}$  (from right to left). As shown in Fig. 15, the steady solution of the spatial distribution of the current and its corresponding velocity potential on the free surface are obtained through a program using boundary element methods. On the bar crest the current velocity is  $-0.8090 \text{ m/s}$ , the setdown of surface elevation is  $-0.0319 \text{ m}$ . According to linear theory only waves with a period larger than  $3.35 \text{ s}$  can be expected to pass the bar without being blocked by the current.

A sinusoidal wave train propagation from left to right on top of the steady current has been imposed. The incoming wave has a period of  $2.0 \text{ s}$  and an initial height of  $0.002 \text{ m}$ . According to linear theory this wave are expected to be blocked where the Froudes number  $F_c = U/\sqrt{gd}$  is  $-0.475$ , where  $d$  is the local water depth. This location is found at  $x = 36.78 \text{ m}$ , where the water depth of the initial steady current from the free surface is  $0.203 \text{ m}$ .

### 6.3. Results of simulation

The computed surface elevations are shown in Figs. 16–22 for different instants during the simulation.

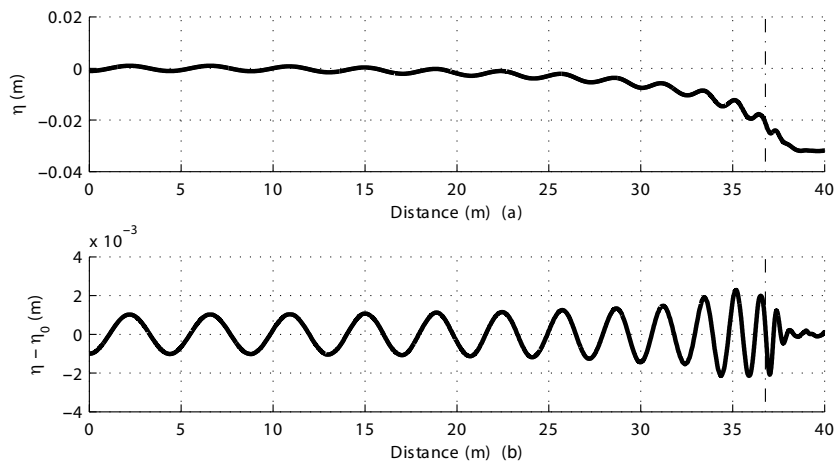


Fig. 16. Spatial distribution of surface elevation with and without setdown from current,  $t = 35$  s.

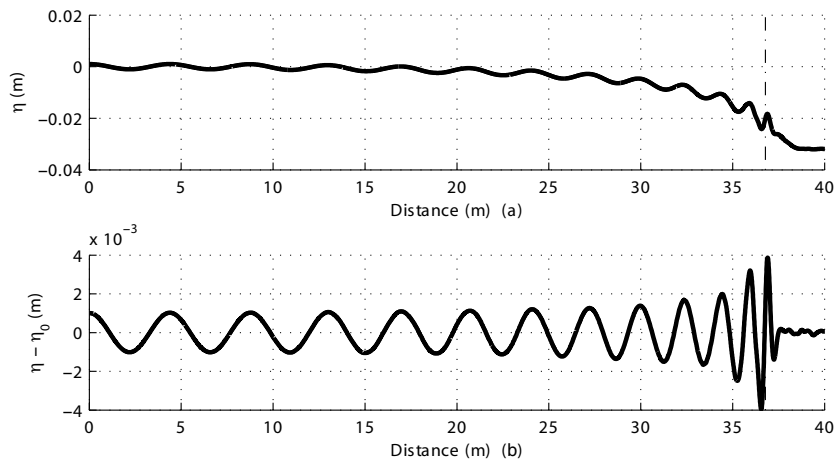


Fig. 17. Spatial distribution of surface elevation with and without setdown from current,  $t = 38$  s.

In Fig. 16, the incoming wave train has just reached the area with strong currents and there is yet no sign of blocking. In Fig. 17, the wave amplitude increases rapidly, implying that the wave energy begins to accumulate. In Fig. 18, the reflected wave has been generated and can be observed in a narrow zone.

From Figs. 19 to 22, the wave amplitude increases to 10 times of that of the incident wave, while the reflected waves are kept in traveling backward. For the reflected waves, the effects of the opposing “original wave” together with the accumulated wave energy will make them shorter and steeper. In reality, those short wave will be rapidly dissipated by surface tension and viscosity ([Trulsen and Mei, 1993]). In the simulation, the steep and short reflected waves demand very fine spatial and temporal resolution, if no dissipation is applied. No dissipation is imposed in the present computation.

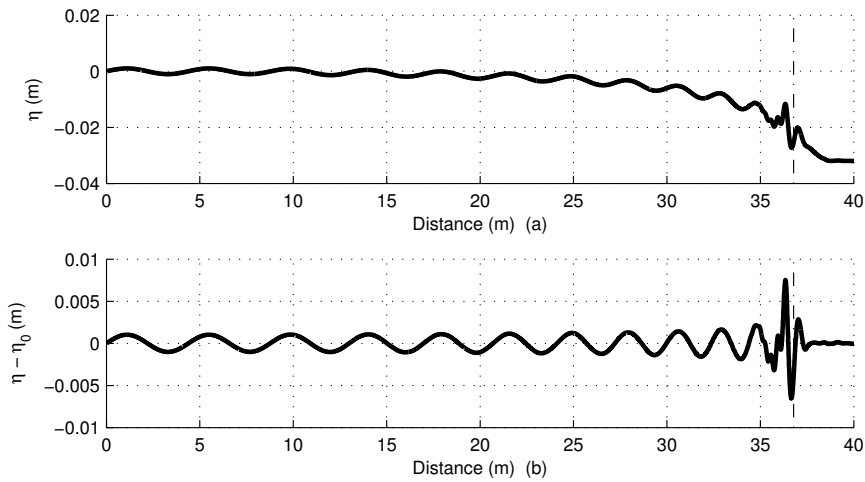


Fig. 18. Spatial distribution of surface elevation with and without setback from current,  $t = 42.5$  s.

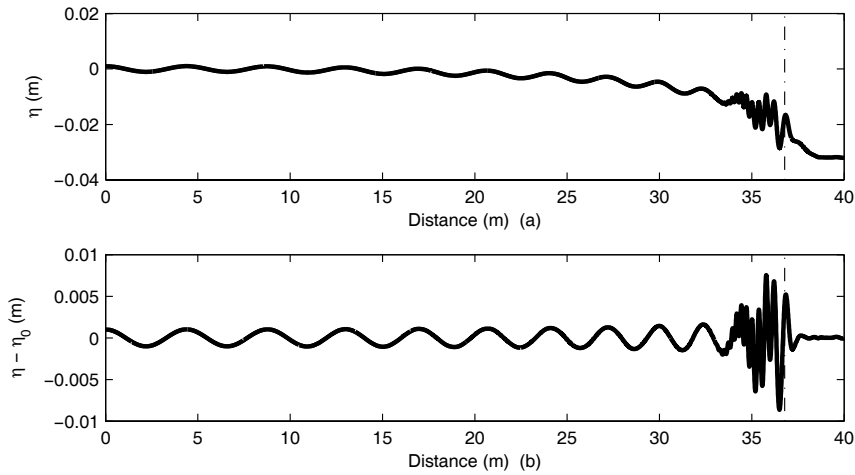


Fig. 19. Spatial distribution of surface elevation with and without setback from current,  $t = 50$  s.

The results of simulation shown here indicate that the model not only accurately predicts the location of the blocking point, but also gives a lucid description of the wave structure in the blocking zone (the zone near the blocking point). It is believed that the stability of the model for simulating the wave blocking phenomenon can be improved by introducing a certain wave breaking model.

### 7. Conclusion

In this study, a new set of equations based on the spatial-temporal separation conception is established through the Galerkin Chebyshev spectral approach on the vertical direction. The 1DH version of this set of equation has been implemented

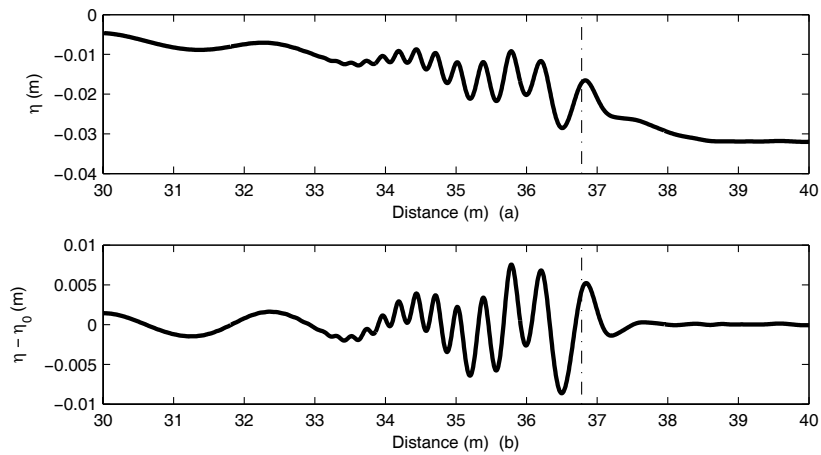


Fig. 20. Spatial distribution of surface elevation with and without setdown from current,  $t = 50$  s.

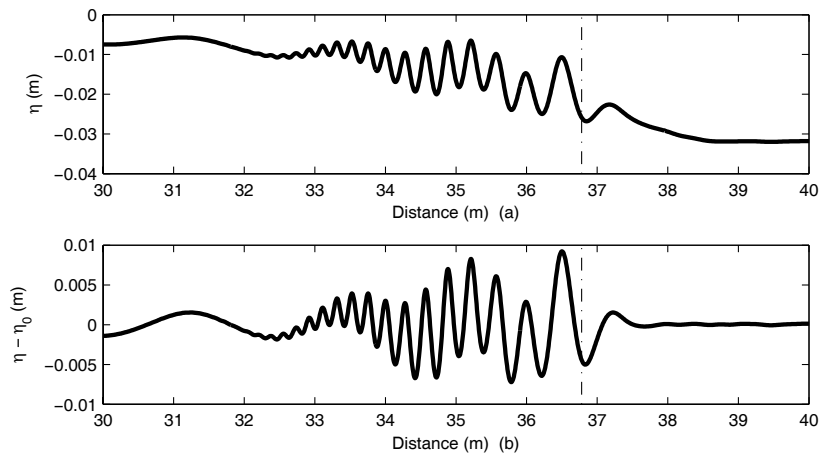


Fig. 21. Spatial distribution of surface elevation with and without setdown from current,  $t = 55$  s.

and verified with theoretical and experimental data. The model is proved to be of high accuracy with moderate cost of computational resources and time.

The model can describe most of the wave and current motions of the potential flow, before the wave overturn and/or breaking. All the nonlinear characteristics have been retained in this model. The dispersion relation of the model is also verified by the simulation of harmonic generation of waves propagating over a submerged bar.

With this model, the wave blocking phenomenon in wave-current interaction has been studied. The results of simulation indicate that the location of blocking point determined by the linear wave theory is accurate for nonlinear phenomenon, while the nonlinear wave structure in the blocking zone is also observed. Besides the above success, several issues emerged during the development of the model.

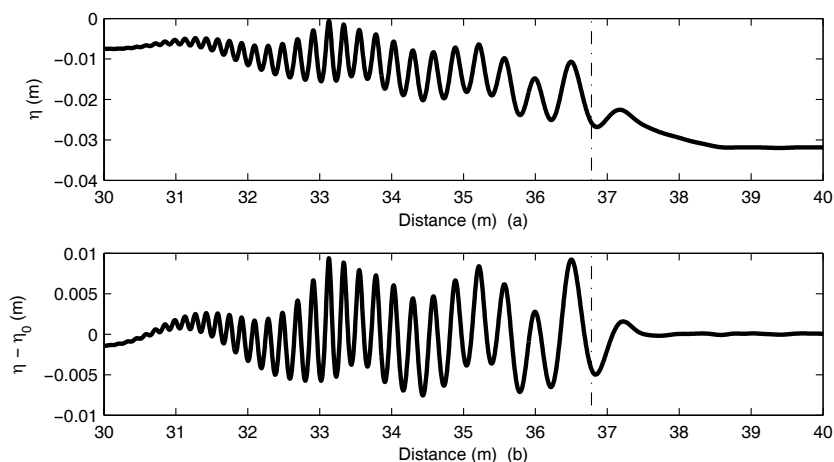


Fig. 22. Spatial distribution of surface elevation with and without setdown from current,  $t = 65$  s.

- (1) An incident wave boundary condition which is able to deal with the reflected wave is necessary in order to simulate the flow pattern around coastal structures.
- (2) 2DH version of the numerical model is expected in order to be applied to real problems.
- (3) A breaking wave model is needed for further simulation.

## References

- Beji, S. & Battjes, J. A. [1965] "Experimental investigation of wave-propagation over a bar," *Coastal Engineering* **19**, 151–162.
- Chen, Q., Madsen, P. A., Sørensen, O. R. & Basco, D. R. [1996] "Boussinesq equations with improved doppler shift and dispersion for wave/current interaction," in *Proc. 25th Int. Conf. on Coastal Eng., ASCE*, pp. 1060–2073.
- Dean, R. G. [1965] "Stream function representation of nonlinear ocean waves," *J. Geophys. Res.* **70**(18), 4561–4572.
- Isobe, M. [1994] "Time dependent mild slope equations for random waves," in *Proc. 24th Int. Conf. on Coastal Eng., ASCE*, pp. 305–325.
- Larsen, J. & Dancy, H. [1983] "Open boundaries in short-wave simulations — A new approach," *Coastal Engineering* **7**(3), 285–297.
- Longuet-Higgins, M. S. & Stewart, R. W. [1961] "The changes in amplitude of short gravity waves on steady non-uniform currents," *J. Fluid Mech.* **10**, 529–549.
- Luth, H. R., Klopman, G. & Kitou, N. [1961] "Kinematics of waves breaking partially on an offshore bar; LDV measurements for waves with and without a net onshore current," *Delft Hydraulics Report, H1573*, Delft Hydraulics, The Netherlands.
- Madsen, P. A. [1999] "A review of boussinesq-type equations for surface gravity waves," *Advances in Coastal and Ocean Engineering*, Vol. 5, Chapter 1 (World Scientific), pp. 1–89.
- Mei, C. C., Stiassnie, M. & Yue, D. K. P. [2005] *Theory and Application of Ocean Surface Wave Part 2: Nonlinear Aspects* (World Scientific).
- Nadaoka, K., Beji, S. & Nakagawa, Y. [1994] "A fully dispersive nonlinear wave model and its numerical solution," in *Proc. 24th Int. Conf. on Coastal Engg., ASCE*, pp. 427–441.
- Nwogu, O. [1993] "Alternative form of boussinesq equations for nearshore wave propagation," *J. Waterways, Port, Coastal, Ocean Engrg., ASCE* **119**(6), 618–638.

- Ohyama, T. & Nadaoka, K. [1991] "Development of a numerical wave tank for analysis of nonlinear and irregular wave field," *Fluid Dynamics Res.* **8**(5–6) (November) 231–251.
- Phillips, O. M. [1977] *The Dynamics of the Upper Ocean* (Cambridge Univ. Press).
- Peregrine, D. H. [1967] "Long waves on a beach," *J. Fluid Mech.* **27**, 815–820.
- Peregrine, D. H. & Thomas, G. P. [1979] "Finite-amplitude deep-water waves on currents," *Phi. Trans. Roy. Soc. London* **292**, 371–390.
- Shuto, N. [1974] "Nonlinear long waves in a channel of variable section," *Coastal Engineering in Japan* **17**, 1–12.
- Shyu, J. H. & Phillips, O. M. [1990] "The blockage of gravity and capillary waves by longer waves and currents," *J. Fluid Mech.* **217**, 115–141.
- Shyu, J. H. & Tung, C. C. [1999] "Refraction of oblique waves by currents: analytical solutions and their application to numerical computations," *J. Fluid Mech.* **396**, 143–182.
- Smith, R. [1975] "The reflection of short gravity waves on a non-uniform current," *Math. Proc. Camb. Phil. Soc.* **78**, 517–525.
- Stiassnie, M. & Peregrine, D. H. [1980] "Shoaling of finite-amplitude surface-waves on water of slowly-varying depth," *J. Fluid Mech.* **97**, 783–805.
- Trulsen, K. & Mei, C. C. [1993] "Double reflection of capillary/gravity waves by a non-uniform current: A boundary-layer theory," *J. Fluid Mech.* **251**, 239–271.
- Wei, G. & Kirby, J. T. [1995] "Time-dependent numerical code for extended boussinesq equations," *J. Waterways, Port, Coastal, Ocean Engrg., ASCE* **121**, 251–261.
- Zakharov, V. E. [1968] "Stability of periodic waves of finite amplitude on the surface of a deep fluid," *J. Appl. Mech. Tech. Phys. (Eng. transl.)* **2**, 190–194.